



This is a repository copy of *Semi-flooded cooling for high torque density modular permanent magnet machines*.

White Rose Research Online URL for this paper:

<https://eprints.whiterose.ac.uk/208578/>

Version: Published Version

Article:

Zhang, W., Li, G.-J. orcid.org/0000-0002-5956-4033, Zhu, Z.-Q. et al. (2 more authors) (2024) Semi-flooded cooling for high torque density modular permanent magnet machines. IET Electric Power Applications, 18 (7). pp. 756-765. ISSN 1751-8660

<https://doi.org/10.1049/elp2.12432>

Reuse

This article is distributed under the terms of the Creative Commons Attribution (CC BY) licence. This licence allows you to distribute, remix, tweak, and build upon the work, even commercially, as long as you credit the authors for the original work. More information and the full terms of the licence here:

<https://creativecommons.org/licenses/>

Takedown



If you consider content in White Rose Research Online to be in breach of UK law, please notify us by emailing eprints@whiterose.ac.uk including the URL of the record and the reason for the withdrawal request.



eprints@whiterose.ac.uk
<https://eprints.whiterose.ac.uk/>

ORIGINAL RESEARCH

Semi-flooded cooling for high torque density modular permanent magnet machines

W. Zhang¹ | G. J. Li¹  | Z. Q. Zhu¹  | B. Ren² | Y. C. Chong²
¹Department of Electronic and Electrical Engineering, The University of Sheffield, Sheffield, UK

²Motor Design Ltd, an ANSYS Company, 5 Edison Court, Wrexham, UK

Correspondence

G. J. Li.

Email: g.li@sheffield.ac.uk

Funding information

Engineering and Physical Sciences Research Council, Grant/Award Number: EP/T017988/1; Motor Design Ltd, an Ansys company

Abstract

The authors investigate a semi-flooded cooling technology for modular permanent magnet machines using flux gaps (FGs) in alternate stator teeth for extra cooling channels. The investigated machine is separated into stationary and rotational components by a polyether ether ketone sleeve. Liquid is directed into the stationary component to achieve a significant temperature reduction, at the same time, avoiding the liquid leakage into the rotating component that will cause an increase in friction losses. The FGs in the modular machine increase the contact area between coolant and machine components, resulting in better cooling efficiency. Furthermore, the FGs contribute to reduced pressure loss by minimising system flow resistance. The influence of the FG width on improving machine cooling efficiency, lowering machine temperature, and reducing pressure losses is delved. Additionally, the investigation considers the impact of inlet and outlet areas to reveal the influences stemming from fluid expansions and contractions in these regions. Computational fluid dynamics (CFD) modelling is employed to simulate the cooling performances of the investigated machines. In addition, the flow network analysis has also been employed to help understand the fluid behaviour within machines. A series of tests have been carried out to validate the CFD modelling.

KEYWORDS

computational fluid dynamics, cooling, permanent magnet machines, thermal analysis

1 | INTRODUCTION

In recent years, thermal management has gained significant interest in electrical machine designs, driven by increasing demands for high torque and power density electrical machines [1]. A well-designed cooling system efficiently reduces machine temperature, thereby allowing for higher current densities. It also helps improve machine reliability and enhance magnet demagnetisation to withstand capability. Cooling technologies encompass both passive and active cooling methods. Passive cooling methods work without additional pumps or devices to circulate coolant. Some of them aim to improve heat conduction within machines, particularly between the end-windings and the machine housing, for example, potting material [2], phase change material [3], and different liquids [4–6]. Others focus on improving heat convection and radiation at

the surface of machine components, for example, heat guides [7] and finned housing [8].

On the other hand, active cooling methods involve the incorporation of additional pumps or devices to establish either a closed-loop coolant circulation or throughflow ventilation for machine cooling. One of the widely used cooling methods for active cooling is the forced air cooling method that employs a fan or a blower to create airflow. In comparison to passive cooling systems, forced air cooling systems significantly enhance thermal convection. Various machine designs utilise fans in different locations to generate different airflow patterns. For example, the totally enclosed fan cooled (TEFC) machines implement a fan outside the totally enclosed machine [9–13]. Moreover, inner fan blades can also be employed and fixed to the shaft for TEFC machines [14, 15]. Totally enclosed fan cooled machines offer advantages such as reduced acoustic

This is an open access article under the terms of the [Creative Commons Attribution](https://creativecommons.org/licenses/by/4.0/) License, which permits use, distribution and reproduction in any medium, provided the original work is properly cited.

© 2024 The Authors. *IET Electric Power Applications* published by John Wiley & Sons Ltd on behalf of The Institution of Engineering and Technology.

noise and lower maintenance cost. However, the totally enclosed frame design limits the cooling efficiency of forced cooling systems. To address this limitation, a new machine configuration, known as a throughflow ventilation machine has been introduced [16, 17]. In throughflow ventilation machines, air is continuously drawn from the surrounding environment into the machines without going through recirculation. However, this exposure to the surrounding environment means that ventilated machines are vulnerable to contaminants.

Liquids are another category of coolants in machine cooling. Typically, liquid cooling systems tend to offer better cooling efficiency than gas cooling systems due to higher thermal conductivity and density. Amongst the liquid cooling technologies, indirect forced liquid cooling technology is widely used, not only for its perfect cooling efficiency but also because it prevents direct contact between the coolant and machine components, thereby avoiding potential corrosion issues. These are pivotal for safety-critical applications. The indirect forced liquid cooling methods include housing water jacket [18], dedicated liquid cooling pipe [19], and additive manufactured heat guides [20].

In contrast to indirect forced liquid cooling systems, direct forced liquid cooling technologies bring the coolant closer to the heat sources, typically the stator iron losses and winding copper losses. Thus, it could have higher cooling efficiency than the indirect forced liquid cooling. Semi-flooded cooling is one of the direct forced liquid cooling technologies, where the coolant is forcibly directed through the components, typically the stationary components such as the stator and windings. This approach involves several flow pathways, as shown in Figure 1a. These flow paths include annular gaps between stator and housing—stator ducts [21], stator axial ducts—flux gaps (FGs) [22], gaps between each conductor in slots—slot gaps [23], and gaps between tooth tips (slot openings) for semi-closed slots [22]. It is worth noting that the viscosities of the coolants employed in semi-flooded cooling systems are typically higher than that of air. Therefore, to prevent an increase in friction losses and coolant leakage, a sleeve is employed to separate the machine into an oil-flooded stator part and an oil-free rotor part, as shown in Figure 1b.

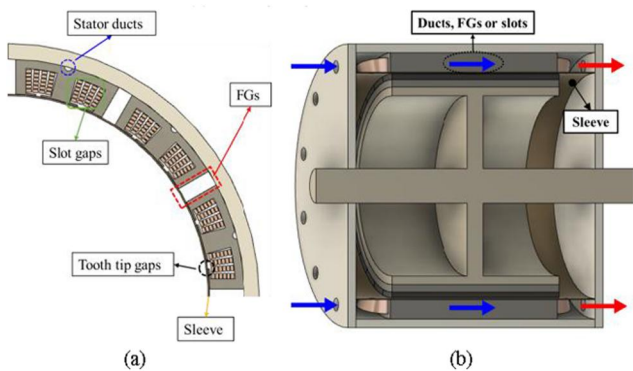


FIGURE 1 (a) Layout of flow pathways in the stator and (b) coolant flow for an electrical machine with direct forced liquid cooling.

In this paper, a direct forced liquid cooling method, known as semi-flooded cooling, is employed to a modular machine as shown in Figure 2. Compared with the conventional permanent magnet (PM) machine, the modular machine achieves higher torque/power density due to three effects, that is, flux focussing effect, improved winding factor and improved airgap flux density [24]. Moreover, FGs are also utilised as extra coolant pathways. The heat transfer and flow profile are investigated using 3D computational fluid dynamics (CFD) modelling in this paper. The results show that extra heat convection occurs in FGs, resulting in a significant reduction in machine temperatures. In addition, the presence of FGs reduces flow resistance for the whole machine, leading to lower pressure losses. The reduction in pressure losses becomes more significant as the FG width increases. Moreover, the pressure losses at different machine components are investigated in this paper to fully reveal the impact of FGs on cooling efficiency. The influence of inlet and outlet areas is also investigated in this paper to demonstrate the influence of coolant expansions and contractions.

2 | COMPUTATIONAL FLUID DYNAMICS MODELLING AND MACHINE SPECIFICATION

2.1 | Computational fluid dynamics modelling and flow network analysis

For the forced air and liquid cooling systems, the CFD modelling is the most popular method for investigating their fluid dynamics and heat transfers. The CFD software package ANSYS-CFX has been used for the research in this paper. It is worth noting that the Reynolds-average Navier–Stokes approach, incorporating the shear stress transport $k-\omega$ model, is employed to address the turbulent flow problem in an electrical machine. This CFD modelling strikes a trade-off between model accuracy and computational efficiency. Furthermore, to reduce the computational burden, the moving

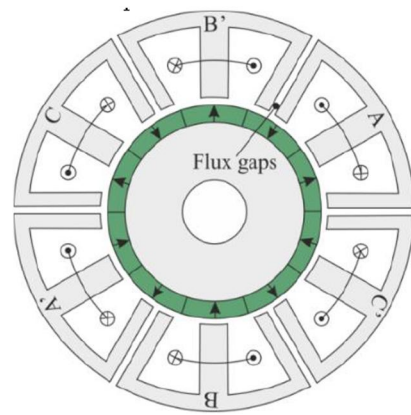


FIGURE 2 Cross-section of the investigated modular machine with flux gaps (FGs).

reference frame, also known as the “frozen rotor”, is employed for steady-state analysis of the rotating machines.

The CFD modelling is powerful but sometimes quite time-consuming. Flow network analysis [25] is another method to predict the local flow velocity and to understand the flow profile. The governing equations of the flow network analysis describe the parabolic relationship between the pressure losses Δp and the volumetric flow rate Q .

$$\Delta p = R_f Q^2 \quad (1)$$

where R_f represents the system flow resistance, expressed as

$$R_f = \frac{k_f \cdot \rho}{2 \cdot A^2} \quad (2)$$

where A is the cross-sectional area of the coolant path, k_f is the dimensionless pressure loss coefficient caused by (1) changing in flow conditions, for example, expansions, contractions, and bends; and (2) fluid friction at wall surface. The properties of coolant such as viscosity and density, topologies of the machines and the cooling system, and the conditions of the machines such as rotor speed are all factors that affect k_f [14].

2.2 | Machine specifications

Compared with a conventional non-modular surface mounted permanent magnet (SPM) machine, the FGs introduced in the modular SPM machine provide an additional degree of freedom for cooling design. In this paper, a semi-flooded oil cooling system is introduced for the modular SPM machine, as shown in Figure 3. The machine specification is listed in Table 1, which is the same for the non-modular machine. For a fairer comparison and to show the improved cooling efficiency with FGs, the losses of both machines are kept the same, that is, the uniformly distributed losses within PMs, stator iron, rotor iron, endwinding and coil active are 249, 799, 60, 90, and 268 W, respectively. The thermal properties of the machine components

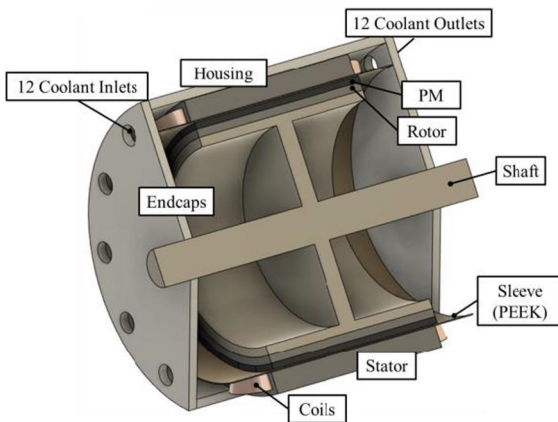


FIGURE 3 Cut away view of the modular SPM machine with forced liquid cooling. SPM, surface mounted permanent magnet.

are listed in Table 2, and the properties of coolant are listed in Table 3. It is worth noting that Hashin and Shtrikman approximation [26] is employed to calculate the anisotropic thermal conductivity of the windings. The slot fill factor is assumed to be 0.4 for all the investigated machines, and the conductivity that is vertical to the current direction is 0.65 W/m/K, while the conductivity that is parallel to the current direction is 160 W/m/K. The average density is 4269 kg/m³ and the average specific heat capacity is 1174 J/kg/K.

12 inlets and 12 outlets are positioned at the same locations on both endcaps, as shown in Figure 3, that is, each stator segment has one inlet and one outlet. The disc-shaped shaft is designed, which helps reduce the mass of the rotor. A poly-ether ether ketone is employed as a sleeve to separate the machine into an oil-flooded stator part and an oil-free rotor part to avoid liquid leakage and friction losses. For the forced cooling systems, the gravitational effect has been neglected. Therefore, the circumferential symmetry of the modular SPM machine leads to a circumferentially symmetrical distribution of flow field and heat transfer. Thus, a one-twelfth (30°) segment is selected for the 3D CFD modelling, as shown in Figure 4. This can significantly reduce the computation time. It is worth noting that the axial domain lengths both upstream and downstream of the machine are around 2 times and 3.5 times the machine length to achieve a fully developed flow

TABLE 1 Parameters of modular SPM machine.

Slot number	24	Rotor outer radius (mm)	129.4
Pole number	28	Rotor yoke thickness (mm)	8.6
Stator outer radius (mm)	154	Stack length (mm)	210
Stator yoke height (mm)	5.6	Housing thickness (mm)	10
Tooth width (mm)	13.2	DC voltage (V)	800
Flux gap width (mm)	10	Rated phase current (I_{peak})	100
Airgap length (mm)	2	Number of turns per coil	10
Magnet thickness (mm)	6.6	Rate speed (rpm)	1500

Abbreviations: DC, direct current; SPM, surface mounted permanent magnet.

TABLE 2 Properties of machine solid components.

	Housing	Rotor/stator	Magnet	Shaft
ρ (kg/m ³)	2790	7650	7500	7800
λ (W/m/K)	168	30	7.6	52
c (J/kg/K)	833	460	7500	460

Note: ρ , λ and c denote the density, thermal conductivity, and specific heat capacity, respectively.

TABLE 3 Properties of the coolant.

Density (kg/m ³)	879
Thermal conductivity (W/m·K)	0.1731
Dynamic viscosity (Pa·s)	0.046
Specific heat capacity (J/kg/K)	1.685×10^3

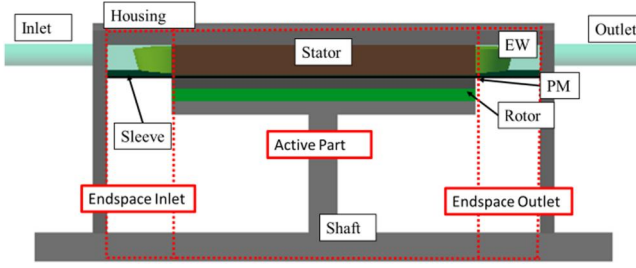


FIGURE 4 Computational fluid dynamics (CFD) model of the modular SPM machine with semi-flooded oil cooling, SPM, surface mounted permanent magnet.

profile. This can prevent the model from experiencing unwanted ‘backflow’ that can cause poor convergence and inaccurate results.

3 | RESULTS AND DISCUSSIONS

Based on the conditions and assumptions detailed in previous sections, a CFD model for the modular SPM machine with semi-flooded oil cooling system has been established. It is worth noting that the convection coefficient at the outer surface of the housing, endcaps and shaft are natural convection, and a value of $8 \text{ W/m}^2/\text{K}$ is used, while the reference temperature for those surfaces is 20°C . The static pressure loss between the inlet and outlet is constant, which is equal to 1000 Pa , and the inlet coolant temperature is 65°C , which is similar to the mainstream coolant temperature used in electrical vehicles (EV). A smooth and no-slip wall is identified for the whole machine surface.

In electrical machines, the convection coefficient is a critical parameter for investigating their thermal performance. The convection coefficient (h_c) can be calculated according to CFD modelling as follows:

$$h_c = \frac{q''_{i,ave}}{T_{wi,ave} - T_{bulk}} \quad (3)$$

where $q''_{i,ave}$, $T_{wi,ave}$, and T_{bulk} are the average heat flux, average wall temperature, and average temperature of coolant for the calculated region.

The coolant velocity distribution and temperature distribution are shown in Figures 5 and 6. Due to its circumferential symmetry, one-fourth (90°) segment is used to show the full flow and thermal profiles, particularly in the FGs. The fluid friction and flow condition change (expansions, contractions, and bends) inside the machine result in the variation of coolant flow velocity in different machine regions. The coolant velocity in the end-space inlet and outlet regions (see Figure 4) is low, but higher velocity can be observed in FGs region, as shown in Figure 5. The heat generated by the windings (copper loss) and the stator iron core (iron losses) is directly removed by the coolant oil. However, the heat generated by the rotor PMs can only be dissipated by convection through the airgap (to the stator) and by conduction through the shaft (to the

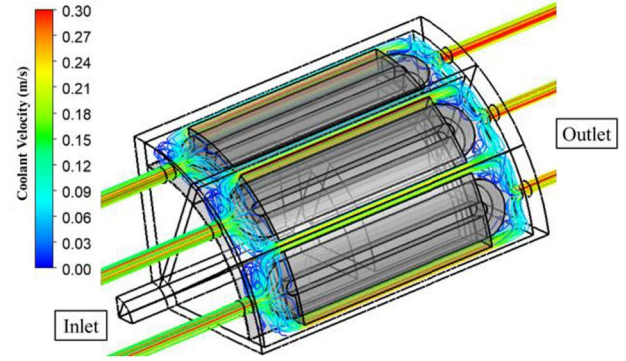


FIGURE 5 Coolant velocity streamline of the modular SPM machine with a flux gap (FG) width of 10 mm . SPM, surface mounted permanent magnet.

environment). Significant temperature reductions for the stator iron core and the windings can be achieved by the semi-flooded cooling technology, as shown in Figure 6. For example, compared with oil-immersed cooling (no oil pump to provide axial flow), employing semi-flooded cooling technology can reduce the maximum winding temperature by around 100°C . Based on (3), the convection coefficient distribution on the surfaces of the stator and end-winding are shown in Figure 7. It is worth noting that the reference temperature (T_{bulk}) of the coolant is 65°C .

3.1 | Influence of flux gap width

According to (2), increasing the cross-sectional area of the coolant path can significantly reduce the system flow resistance. This means that the width of the FG can directly affect the cooling efficiency of the semi-flooded cooling system. Thus, the influence of FG width on the flow profile has been investigated in this section. It is worth noting that to understand the influence of the FG width, the heat sources in the stator iron, windings and PMs for different FG widths will be kept the same. A constant pressure loss of 1000 Pa between the inlet and outlet will be maintained for different FG widths. It is worth noting that the FGs are the only coolant path for the semi-flooded cooling system that are designed in this section. Therefore, the coolant will be fully obstructed when the FG width is 0 mm , corresponding to a non-modular machine. Hence, the cooling system is an oil-immersed cooling system that does not have axial flow when the FG width is 0 mm . In this paper, considering the manufacturing complexity and tolerance, a minimum FG width of 3 mm for the modular machines has been selected. It is therefore worth noting that the semi-flooded oil cooling system designed in this paper may not be suitable for modular machines with narrower FGs unless higher pressure loss is acceptable.

The change of system flow resistance affects the relationship between the pressure loss and the flow rate as described by (1). If the pressure loss is constant, increasing the FG width

can reduce the flow resistance and improve the volumetric flow rate as shown in Figure 8. However, this improvement becomes gradually insignificant when the FG width keeps increasing.

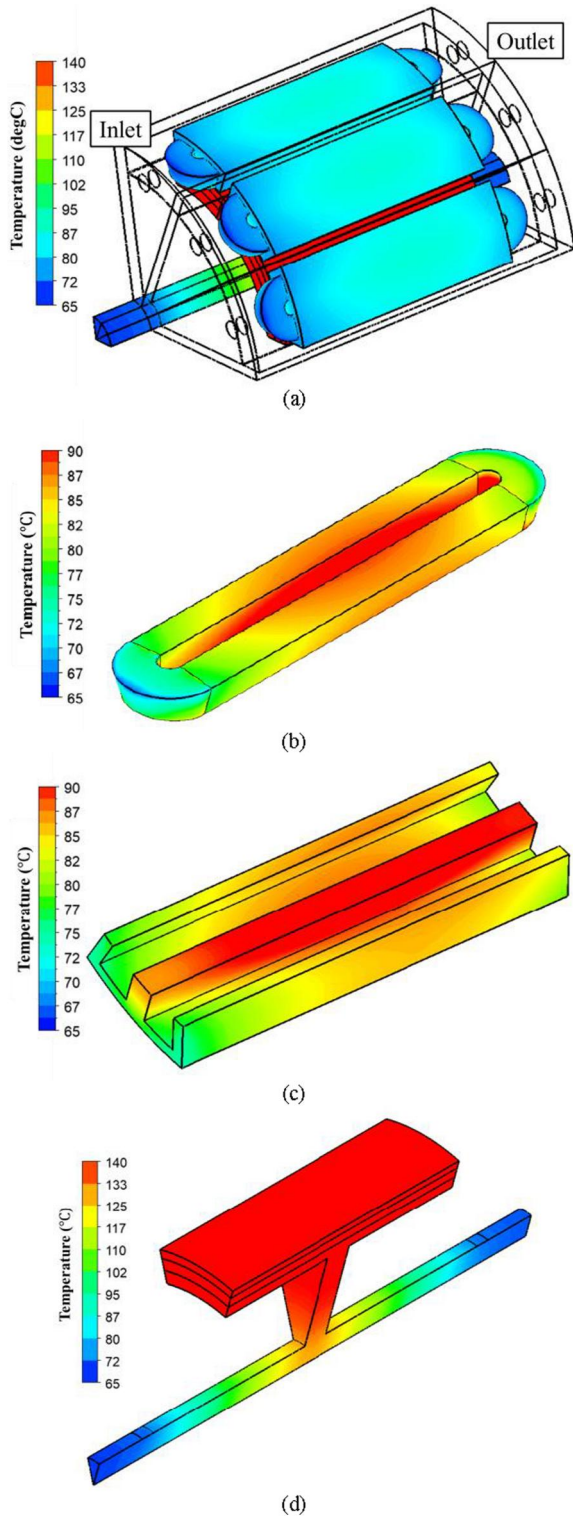


FIGURE 6 Temperature distribution of (a) entire machine, (b) coil, (c) stator segment, and (d) rotor for the modular SPM machine with a flux gap (FG) width of 10 mm. SPM, surface mounted permanent magnet.

When the FG width increases, the coolant velocity changes as shown in Figure 9. Benefited from the rapid increase of the volumetric flow rate as shown in Figure 8, the coolant velocity in the FG region also increases when the FG width increases until it reaches 8 mm. However, the increased FG width also leads to a larger cross-sectional area, which has a negative impact on the coolant velocity. Thus, when the FG width is

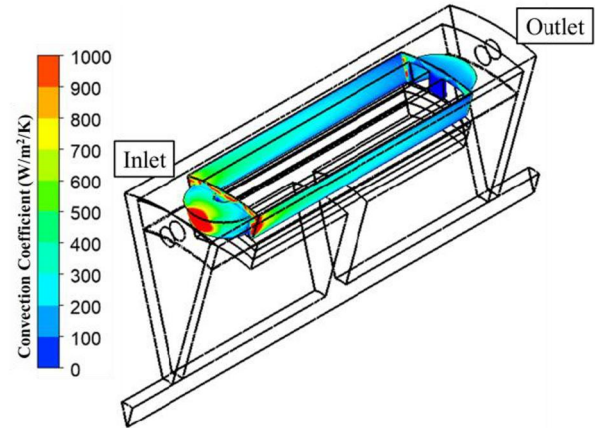


FIGURE 7 Convection coefficient distribution at the surfaces in contact with the coolant oil for the modular SPM machine with a flux gap (FG) width of 10 mm. SPM, surface mounted permanent magnet.

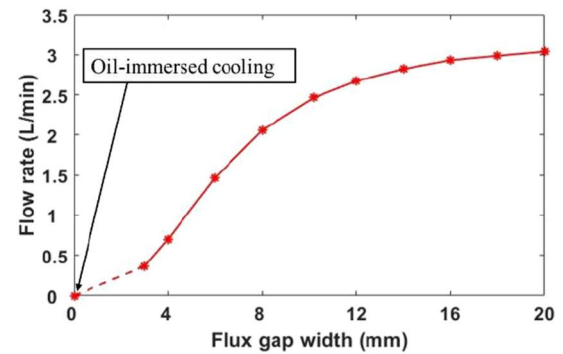


FIGURE 8 Flow rate versus different flux gap (FG) widths for the investigated modular machines with a constant static pressure loss of 1000 Pa.

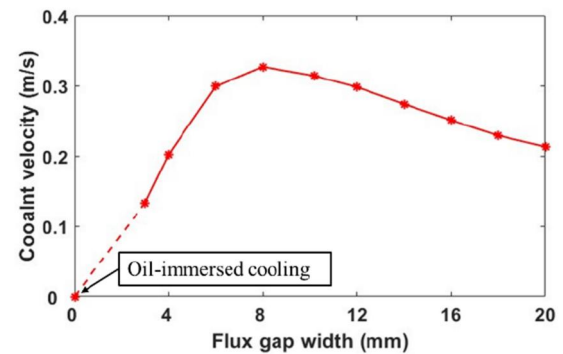


FIGURE 9 Coolant velocity at the centre of the flux gap (FG) versus different FG widths for the investigated modular machines with a constant static pressure loss of 1000 Pa.

larger than 8 mm, this negative impact becomes more dominant and the coolant velocity in the FGs gradually reduces.

The machine has been divided into three regions, that is, end-space inlet region, end-space outlet region and active part, as shown in Figure 4. The total pressure loss of the whole machine is the sum of all pressure losses in each region. The pressure losses at each region are shown in Figure 10. When the FG width is small, the dimensionless pressure loss coefficient at the active part, that is, FGs region, is much larger than those in the other two regions. According to the flow network analysis, most pressure loss is in the FG region. When the FG width increases, the dimensionless pressure loss coefficient significantly reduces. As a result, more pressure loss comes from the end-space regions. It is worth noting that the dimensionless pressure loss coefficients for the fluid channel expansions and contractions are different [25], as shown in Figure 11, and the pressure losses in the end-space inlet region and outlet region are not the same. More details about the dimensionless pressure loss coefficients for expansion and contractions can be seen in section III-B.

The average convection coefficients at the surfaces of FGs, inlet and outlet end-windings have been calculated by (3) for different FG widths, as shown in Figure 12. It demonstrates that when FG width increases, the convection coefficient in the FGs increases first. This is because a larger coolant velocity is

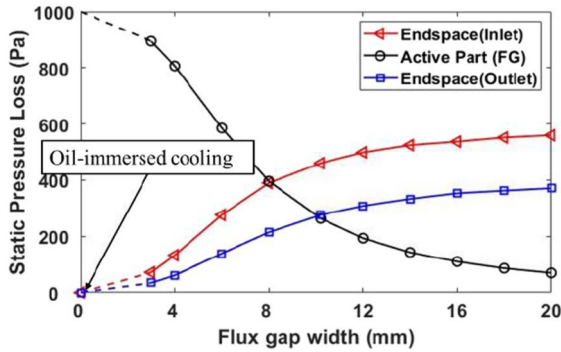


FIGURE 10 Pressure losses at end-space inlet region, end-space outlet region, and active part versus flux gap (FG) widths for the investigated modular machines with a constant total static pressure loss of 1000 Pa.

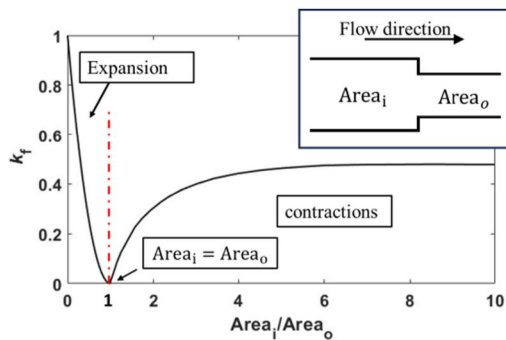


FIGURE 11 Dimensionless pressure loss coefficient (k_f) caused by sudden expansions or contractions of fluid channel [25].

available, as shown in Figure 9. However, when the FG width increases further, the convection coefficient reduces due to the lower coolant velocity caused by the larger cross-sectional area. In the meantime, more pressure loss occurs in the end-space regions, which leads to an increase in the convection coefficient in the end-space region, particularly at the surface of inlet end-winding which directly faces the inlet flow.

The maximum temperatures of the end-windings in the inlet or outlet regions, active coil and PM are shown in Figure 13. The stationary components, that is, end-windings in

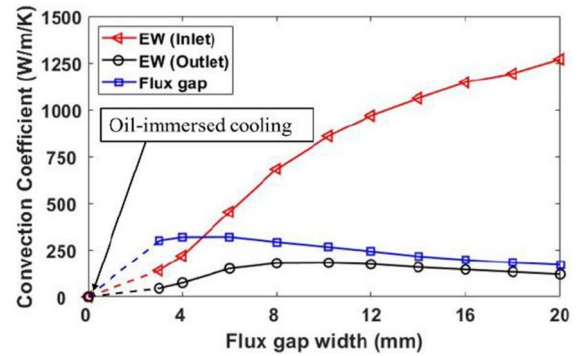


FIGURE 12 Convection coefficients on surfaces of end-winding in end-space inlet and outlet regions, and flux gap (FG) region versus FG widths for the investigated modular machines with a constant total static pressure loss of 1000 Pa.

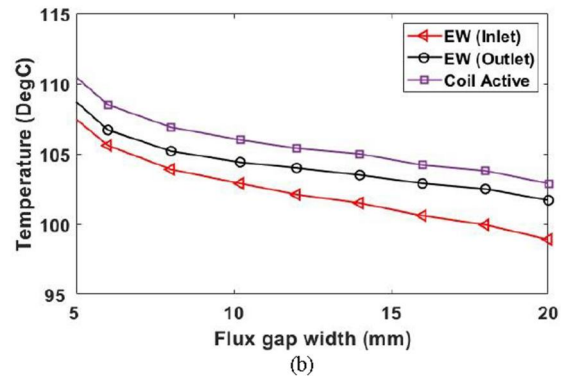
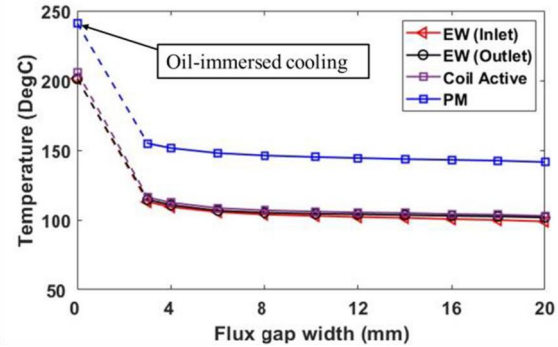


FIGURE 13 Maximum temperatures at end-windings in end-space inlet and outlet regions, active coil and permanent magnet (PM) versus flux gap (FG) widths. (a) Temperatures for all machine components and (b) zoom-in view of the stationary components.

inlet or outlet regions and active coil, benefit much more from the semi-flooded cooling technology than the rotating components, that is, PM. Same as the flow rate, the machine temperature reduces when the FG width increases. However, the reduction rate of the temperature becomes smaller when the FG width is large.

3.2 | Influence of inlet and outlet areas

According to flow network analysis, the expansions and contractions of fluid lead to additional pressure losses. These pressure losses also follow the pressure loss equation described by (1) and (2). The dimensionless pressure loss coefficients for sudden expansions and contractions are calculated by [25].

$$k_f = \begin{cases} \left(1 - \frac{Area_i}{Area_o}\right)^2 & Area_i < Area_o \\ 0.5 \times \left(1 - \frac{Area_o}{Area_i}\right)^{0.75} & Area_i > Area_o \end{cases} \quad (4)$$

where $Area_i$ and $Area_o$ denote the upstream and downstream areas of the fluid channel, respectively, as shown in Figure 11.

Therefore, when the cross-sectional areas of the inlet and outlet increase and the machine inside the region is constant, $Area_i/Area_o$ for the end-space inlet region (expansion) and $Area_o/Area_i$ for the end-space outlet region (contraction) both tend to be 1. Thus, k_f tends to be 0, as shown in Figure 11. As a result, increasing the cross-sectional area of the inlet/outlet results in lower pressure loss in inlet and outlet regions. And higher flow rate for the whole system can be achieved when the pressure loss is constant, as shown in Figure 14.

Due to the influence of the inlet/outlet area on the flow rate, the convection coefficient and temperature will also be affected by the change in the inlet/outlet area. For example, the inlet and outlet areas increase, and the convection coefficients on the surfaces of different machine components all increase as shown in Figure 15. Additionally, the temperatures on the surfaces of different machine components all reduce, as shown in Figure 16. It is also found that the surface of the end-winding facing the inlet flow benefits more from the increase in the inlet/outlet area.

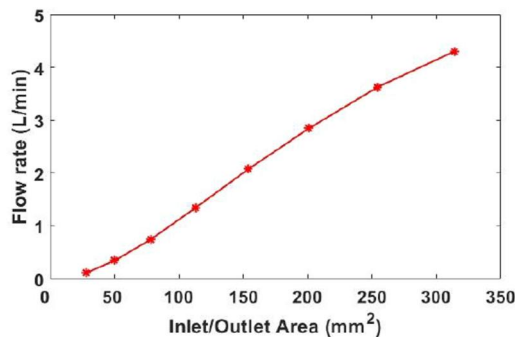


FIGURE 14 Flow rate versus inlet or outlet areas.

4 | EXPERIMENTAL VALIDATION

In order to validate the CFD modelling and predictions in this paper, a motorette representing the modular machine has been manufactured and tested, as shown in Figure 17. The key parameters of this motorette are listed in Table 4. The complete test rig is shown in Figure 18. In the motorette, the FG width is adjustable and can be changed from 2 to 8 mm. The motorette is connected to an oil pump system, and the fluid parameters such as fluid temperature, flow rate and pressure are continuously monitored in real time using an ultrasonic fluid metre SU7200 manufactured by IFM Electronic. The temperature

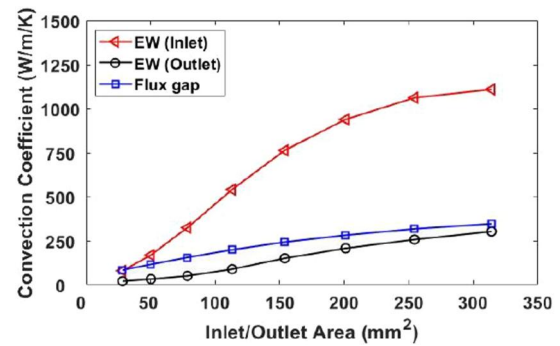


FIGURE 15 Convection coefficients in end-windings in end-space inlet and outlet regions and flux gap (FG) region versus inlet or outlet areas.

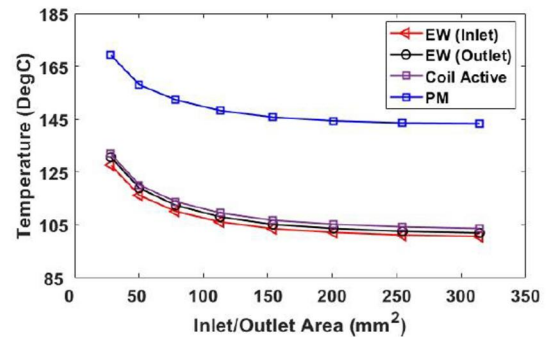


FIGURE 16 Maximum temperatures in end-windings in end-space inlet and outlet regions and active part versus inlet or outlet areas.

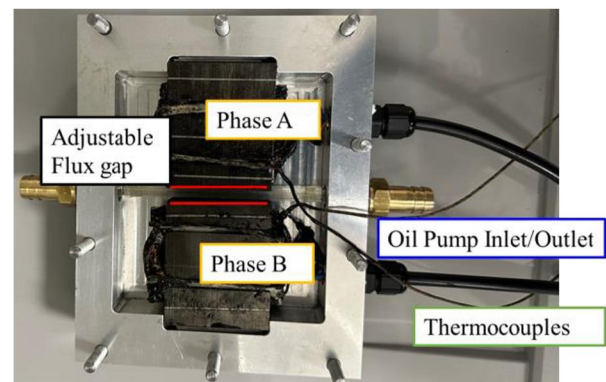


FIGURE 17 The motorette representing the modular machine.

variation of the windings is also monitored in real time using a Pico Technology temperature data logger.

Coolant oils with different volumetric flow rates have been pumped into the motorette, and the pressure losses for different FG widths have been simulated and measured, as shown in Figure 19. Good agreement between the measured and simulated results can be observed. It is worth noting that the oil properties, particularly the dynamic viscosity, are temperature-dependent. They significantly affect the flow rate and pressure drop of the cooling system. Therefore, the pressure losses for all tested objects were measured when the coolant temperature is 20°C. The results also confirmed that the increase of the FG width results in lower system flow resistance and therefore lower pressure losses.

The winding temperature variations for the motorette with 2 and 8 mm FGs have also been measured to compare against the simulation results, as shown in Figure 20. To fully understand the influence of the FGs, the cooling system was operated at the same volumetric flow rate of 5 L/min. The losses for the tests were generated by a dc power supply with a constant current of 10A. It is worth noting that the dynamic viscosity of the coolant changes over time due to temperature

TABLE 4 Parameters of motorette.

Segment number	2	Segment height (mm)	21.5
Stack length (mm)	50	Housing length (mm)	180
Flux gap width (mm)	2~8	Housing width (mm)	140
Segment length (mm)	58.4	Housing height (mm)	26.5
Segment yoke height (mm)	3.7	Inlet/outlet diameter (mm)	12
Segment tooth width	7.1	Number of turns	66

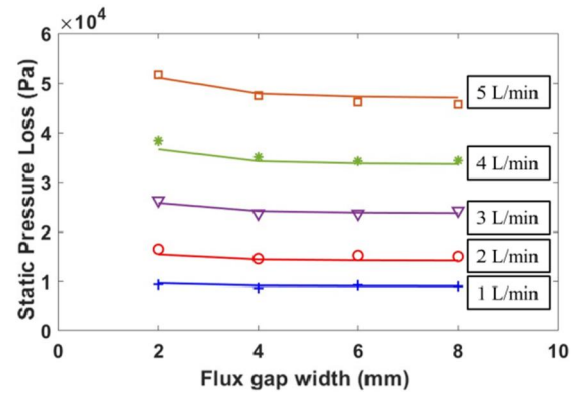


FIGURE 19 Pressure losses of the whole cooling system for the motorette with different flux gap (FG) widths. It is worth noting that the solid lines represent the simulated results, and the dots represent the experimental results.

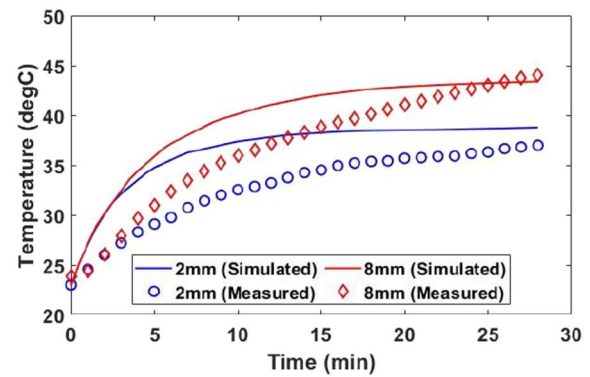


FIGURE 20 Simulated and measured winding temperatures of the motorette with 2 and 8 mm flux gaps (FGs).

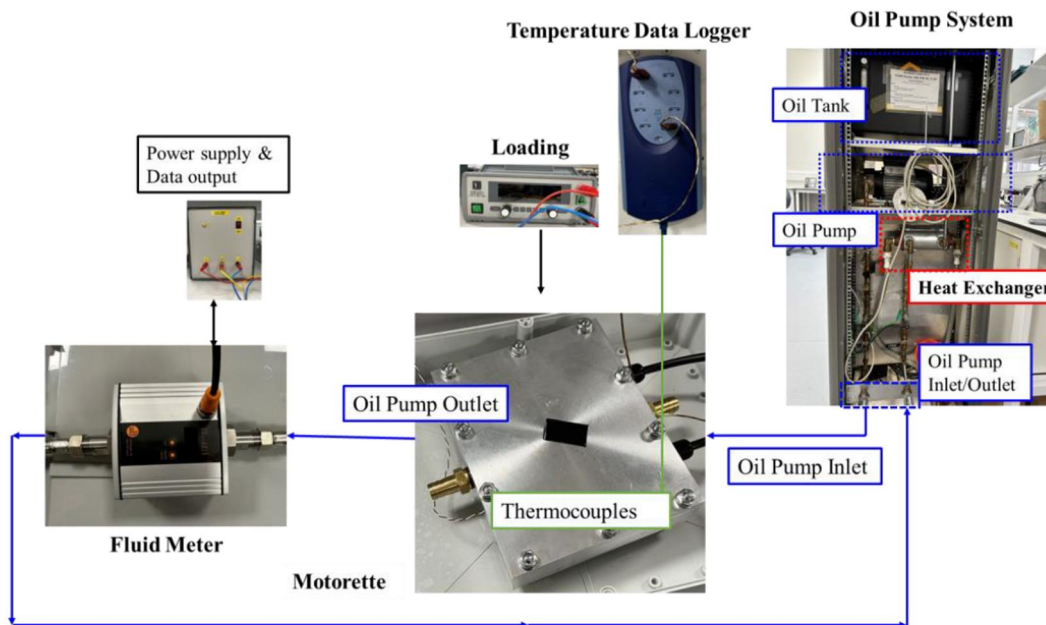


FIGURE 18 Test rig for the semi-flooded oil cooling machine with stator modularity.

rise, causing variations in both the volumetric flow rate and the total pressure loss during the experiments. The test rig operated only until the coolant temperature reached 30°C, and the properties (including dynamic viscosity and thermal conductivity) of the oil are specified at a reference temperature of 30°C for the simulations.

It is found that the measured and simulated temperatures did not match closely, but similar temperature differences were noted for different FG widths. The discrepancy between the measured and simulated results is mainly due to the temperature-dependent viscosity of the cooling oil that has not been considered in the simulations. The temperature of the oil increased from room temperature to 30°C, and its dynamic viscosity reduced. The reduced viscosity led to a gradually increased volumetric flow rate, and therefore the measured temperatures were lower than the simulated ones.

A lower winding temperature was found for the motorette with narrower FGs, attributed to the faster coolant velocity achieved in these FGs. It is worth noting that the advantage of wider FGs was not fully achieved in this experiment. This is because the majority of the pressure loss occurs in other components of the cooling system, such as pipe connections, bent pipes, fluid metres, and heat exchangers, rather than in the motorette itself. Consequently, the reduced flow resistance in the motorette was not as significant as anticipated. However, in practice, the majority of the pressure loss should ideally be situated within the electrical machines to ensure efficient cooling. In such cases, the benefits of FGs in enhancing machine thermal performance would be more pronounced.

5 | CONCLUSION

This paper explores the utilisation of semi-flooded oil cooling in both modular SPM machines and their non-modular counterparts. To assess the cooling efficiencies, understand flow profiles, and evaluate heat transfers, a series of 3D CFD modelling has been conducted. The investigation underscores that the semi-flooded oil cooling system notably decreases machine temperatures, particularly within the stationary components. The study also delves into the impact of the FG width on machine cooling. These gaps, due to their augmented flow path, increased surface area of immersed solid, and reduced flow resistance, contribute to decreased pressure losses, higher convection coefficients, elevated flow rates, and reduced machine temperatures, especially in the case of modular machines. These benefits become more pronounced with wider FGs.

Furthermore, the paper investigates the effects of inlet and outlet area variations in forced cooling technologies. A larger area substantially diminishes the dimensionless pressure loss coefficient resulting from sudden expansions and contractions. This leads to increased flow rates, enhanced convection coefficients, and reduced machine temperatures. Consequently, a larger area is preferred, provided it does not compromise mechanical reliability. The validity of the simulation models and conclusions presented in this paper has been confirmed

through a series of tests using a motorette, which serves as a representative model for the investigated modular machines.

AUTHOR CONTRIBUTIONS

W. Zhang: Conceptualisation; Formal analysis; Investigation; Methodology; Visualisation; Writing – original draft. **G. J. Li:** Supervision; Writing – review & editing. **Z. Q. Zhu:** Writing – review & editing. **B. Ren:** Funding acquisition; Project administration; Resources. **Y. C. Chong:** Funding acquisition; Resources.

ACKNOWLEDGEMENT

This work is partially supported by the UK Engineering and Physical Science Research Council under Grant No. EP/T017988/1 and partially sponsored by Motor Design Ltd, an Ansys company.

For the purpose of open access, the author has applied a Creative Commons Attribution (CC BY) licence to any Author Accepted Manuscript version arising.

CONFLICT OF INTEREST STATEMENT

The authors declare no conflict of interest.

DATA AVAILABILITY STATEMENT

The data that support the findings of this study are available on request from the corresponding author.

ORCID

G. J. Li  <https://orcid.org/0000-0002-5956-4033>

Z. Q. Zhu  <https://orcid.org/0000-0001-7175-3307>

REFERENCES

1. Staton, D., et al.: Cooling of Rotating Electrical Machines: Fundamentals, Modelling, Testing and Design. IET (2022)
2. Polikarpova, M., et al.: Application of potting material for a 100 kW radial flux PMSM. In: 2014 ICEM, pp. 2146–2151. IEEE (2014)
3. T'Jollyn, I., et al.: Measurements on thermal buffering of electric machine peak loads with phase change materials. In: 2022 ICEM, pp. 1934–1940. IEEE (2022)
4. Biasion, M., et al.: A comparison of cryogenic-cooled and superconducting electrical machines. In: 2021 IEEE ECCE, pp. 4045–4052. IEEE (2021)
5. Vaschetto, S., et al.: Nanofluids for rotating electrical machines cooling: perspectives and challenges. In: 2019 21st ECCE Europe, pp. 1–10. IEEE (2019)
6. Karimi Moghaddam, G., et al.: Thermomagnetic liquid cooling: a novel electric machine thermal management solution. In: 2014 IEEE ECCE, pp. 1482–1489. IEEE (2014)
7. Wrobel, R., Hussein, A.: Design considerations of heat guides fabricated using additive manufacturing for enhanced heat transfer in electrical machines. In: 2018 IEEE ECCE, pp. 6506–6513. IEEE (2018)
8. Ulbrich, S., Kopte, J., Proske, J.: Cooling fin optimization on a TEFC electrical machine housing using a 2-D conjugate heat transfer model. IEEE Trans. Ind. Electron. 65(2), 1711–1718 (2017). <https://doi.org/10.1109/tie.2017.2748051>
9. Roffi, M., Ferreira, F.J., De Almeida, A.T.: Comparison of different cooling fan designs for electric motors. In: 2017 IEEE IEMDC, pp. 1–7. IEEE (2017)
10. Boglietti, A., et al.: A simplified thermal model for variable speed self cooled industrial induction motor. In: Conference Record of the 2002

- IEEE Industry Applications Conference. 37th IAS Annual Meeting (Cat. No. 02CH37344), vol. 2, pp. 723–730. IEEE (2002)
11. Valenzuela, M.A., Tapia, J.A.: Heat transfer and thermal design of finned frames for TEFC variable-speed motors. *IEEE Trans. Ind. Electron.* 55(10), 3500–3508 (2008). <https://doi.org/10.1109/tie.2008.928150>
 12. Kral, C., et al.: Comparison of a CFD analysis and a thermal equivalent circuit model of a TEFC induction machine with measurements. *IEEE Trans. Energy Convers.* 24(4), 809–818 (2009). <https://doi.org/10.1109/tec.2009.2025428>
 13. Zhu, Z.Q., Liang, D.: Perspective of thermal analysis and management for permanent magnet machines, with particular reference to hotspot temperatures. *Energies* 15(21), 8189 (2022). <https://doi.org/10.3390/en15218189>
 14. Gai, Y.H., et al.: Cooling of automotive traction motors: schemes, examples, and computation methods. *IEEE Trans. Ind. Electron.* 66(3), 1681–1692 (2018). <https://doi.org/10.1109/tie.2018.2835397>
 15. Mizuno, S., et al.: Development of a totally enclosed fan-cooled traction motor. *IEEE Trans. Ind. Appl.* 49(4), 1508–1514 (2013). <https://doi.org/10.1109/tia.2013.2256872>
 16. Yung, C.: Cool facts about cooling electric motors. In: Industry Applications Society 60th Annual Petroleum and Chemical Industry Conference, pp. 1–10. IEEE (2013)
 17. Fawzal, A.S., et al.: Fan performance analysis for rotor cooling of axial flux permanent magnet machines. *IEEE Trans. Ind. Appl.* 53(4), 3295–3304 (2017). <https://doi.org/10.1109/tia.2017.2675986>
 18. Sato, Y., et al.: Development of High Response Motor and Inverter System for the Nissan LEAF Electric Vehicle. SAE Technical Paper, 0148-7191 (2011)
 19. Madonna, V., et al.: Improved thermal management and analysis for stator end-windings of electrical machines. *IEEE Trans. Ind. Electron.* 66(7), 5057–5069 (2018). <https://doi.org/10.1109/tie.2018.2868288>
 20. Wrobel, R., McGlen, R.J.: Heat pipes in thermal management of electrical machines—A review. *Therm. Sci. Eng. Prog.* 26, 101053 (2021). <https://doi.org/10.1016/j.tsep.2021.101053>
 21. Huang, Z., et al.: Direct oil cooling of traction motors in hybrid drives. In: 2012 IEEE Inter. Elect. Vehicle Conf, pp. 1–8. IEEE (2012)
 22. La Rocca, A., et al.: Thermal management of a high speed permanent magnet machine for an aeroengine. In: 2016 XXII ICEM, pp. 2732–2737. IEEE (2016)
 23. Schiefer, M., Doppelbauer, M.: Indirect slot cooling for high-power-density machines with concentrated winding. In: 2015 IEEE IEMDC, pp. 1820–1825. IEEE (2015)
 24. Li, G.J., et al.: Influence of flux gaps on electromagnetic performance of novel modular PM machines. *IEEE Trans. Energy Convers.* 29(3), 716–726 (2014). <https://doi.org/10.1109/tec.2014.2312429>
 25. Staton, D.A., Cavagnino, A.: Convection heat transfer and flow calculations suitable for electric machines thermal models. *IEEE Trans. Ind. Electron.* 55(10), 3509–3516 (2008). <https://doi.org/10.1109/tie.2008.922604>
 26. Simpson, N., Wrobel, R., Mellor, P.H.: Estimation of equivalent thermal parameters of impregnated electrical windings. *IEEE Trans. Ind. Appl.* 49(6), 2505–2515 (2013). <https://doi.org/10.1109/tia.2013.2263271>

How to cite this article: Zhang, W., et al.: Semi-flooded cooling for high torque density modular permanent magnet machines. *IET Electr. Power Appl.* 1–10 (2024). <https://doi.org/10.1049/elp2.12432>